The CLYC-6 and CLYC-7 response to γ-rays, fast and thermal neutrons

A. Giaz [a], L. Pellegri [a], F. Camera [a,b,*], N. Blasi [a], S. Brambilla [a], S. Ceruti [a,b], B. Million [a], S. Riboldi [a,b], C. Cazzaniga [c,d], G. Gorini [c,d], M. Nocente [c,d], A. Pietropaolo [e], M. Pillon [e], M. Rebai [c], M. Tardocchi [d]

[a] INFN Milano, Via Celoria 16, 20133 Milano, Italy
[b] Università degli Studi di Milano, Physics Department, Via Celoria 16, 20133 Milano, Italy
[c] University of Milano Bicocca, Physics Department, Piazza della Scienza 3, 20126 Milano, Italy
[d] Istituto di Fisica del Plasma, Associazione EURATOM-ENEA-CNR, via Roberto Cozzi 53, 20125 Milano, Italy
[e] Associazione EURATOM-ENEA sulla Fusione ENEA C.R. Frascati, Via E. Fermi 45, 00044 Frascati, Roma, Italy

A B S T R A C T

The crystal Cs_2LiYCl_6:Ce (CLYC) is a very interesting scintillator material because of its good energy resolution and its capability to identify γ-rays and fast/thermal neutrons. The crystal Cs_2LiYCl_6:Ce contains ^{6}Li and ^{35}Cl isotopes, therefore, it is possible to detect thermal neutrons through the reaction ^{6}Li (n, α)t while ^{35}Cl ions allow to measure fast neutrons through the reactions ^{35}Cl(n, p)^{35}S and ^{35}Cl(n, α)^{32}P. In this work two CLYC 1″ × 1″ crystals were used: the first crystal, enriched with ^{6}Li at 95% (CLYC-6) is ideal for thermal neutron measurements while the second one, enriched with ^{7}Li at > 99% (CLYC-7) is suitable for fast neutron measurements. The response of CLYC scintillators was measured with different PMT models: timing or spectroscopic, with borosilicate glass or quartz window. The energy resolution, the neutron-γ discrimination and the internal activity are discussed. The capability of CLYC scintillators to discriminate γ rays from neutrons was tested with both thermal and fast neutrons. The thermal neutrons were measured with both detectors, using an AmBe source. The measurements of fast neutrons were performed at the Frascati Neutron Generator facility (Italy) where a deuterium beam was accelerated on a deuterium or on a tritium target, providing neutrons of 2.5 MeV or 14.1 MeV, respectively. The different sensitivity to thermal and fast neutrons of a CLYC-6 and of a CLYC-7 was additionally studied.

1. Introduction

In the last 15 years, the search for high performing scintillators produced several new materials [1]. In particular, Lanthanum Halide [2–8], Elpasolite [9–17], SrI_2:Eu [1,18], $CeBr_3$ [1,19–20] and Ceramic scintillators [1,21] show better performances than those of the very well-known NaI:Tl, CsI:Tl, BGO or BaF_2 scintillators.

A promising class of scintillators are the Elpasolite, discovered about 10 years ago. The Cs_2LiYCl_6:Ce (CLYC), $Cs_2LiLaCl_6$:Ce (CLLC) and $Cs_2LiLaCl_6$:Ce (CLLB) scintillators belong to this class. They are characterized by a good energy and time resolution, high linearity, especially at low energy. In particular, the CLYC scintillators are characterized by a light yield of ~20 ph/keV, a density of 3.3 g/cm^3 and an energy resolution of less than 5% at 662 keV. They can identify and measure γ rays and neutrons at the same time via pulse shape discrimination (PSD) [9–17,22–27].

The sensitivity to thermal neutrons is given by the well known reaction ^{6}Li + n = ^{3}H + α which has a cross-section of 940 barns [9–12]. The emitted tritium (^{3}H) and the α particles deposit approximately 3.2 MeVee (MeV electron equivalent). The sensitivity of CLYC to fast neutrons, instead, was found to be given by the reactions on ^{35}Cl (^{35}Cl + n = ^{35}S + p and ^{35}Cl + n = ^{32}P + α), which have cross-sections of the order of 100–300 mb [13–16,22–24]. In addition, the energy of the outgoing proton and α particle scales linearly with the kinetic energy of the incident fast neutron [13,15,24]. Therefore, the energy of the incident neutron can be directly deduced from the pulse generated by the detector. This unique capability makes CLYC a very promising scintillator for both γ and neutron spectrocopy in base research and application.

Since the capability of CLYC to detect thermal neutrons is provided by ^{6}Li, the selection of ^{6}Li or ^{7}Li enrichment allows to control the sensitivity of a CLYC scintillator to thermal neutrons. In particular, an enrichment in ^{6}Li (CLYC-6) increases the sensitivity to thermal neutrons while an enrichment in ^{7}Li (CLYC-7) suppresses the sensitivity to thermal neutrons allowing a better detection of fast neutrons.

* Corresponding author at: Università degli Studi di Milano, Physics Department, Via Celoria 16, 20133 Milano, Italy.
E-mail address: franco.camera@mi.infn.it (F. Camera).

It has been shown that the CLYC emission light spectrum is characterized by fast and slow components [16]. The fast component is predominantly induced by γ-rays and it is in the UV part of the spectrum (approximately 220–320 nm). It is generally associated to the CVL (Core to Valence Luminescence) scintillation light which could be partially or totally reabsorbed and re-emitted by Ce dopant. It has been shown [16] that the intensity of CVL is suppressed as temperature increases. However the PSD effectiveness in n–γ identification is not reduced. The medium and slow components of the scintillation light are located in the blue region of the light spectrum (approximately 350–500 nm) and it was shown that they are present in both γ-rays and neutrons induced signals [13–17].

There are in literature several studies on the properties of ^{6}Li enriched detectors (see for example Refs. [9–17]). However there are few works on i) ^{7}Li enriched crystals (almost insensitive to thermal neutrons but good for neutron spectroscopy) [15], ii) the measurement of CLYC internal radiation [9] and iii) the effects in CLYC performances with timing PMT or a quartz window PMT. In the first part of this work (Section 2) we present the general properties of the used CLYC-6 (enriched at 95% of ^{6}Li, as reported in RMD datasheets) and CLYC-7 (with an enrichment of ^{7}Li larger than 99%, as reported in RMD datasheets) scintillators [25]. Both detectors show the typical energy resolution already measured in Refs. [9–14] but slightly better than the one reported in [15]. Section 2.2 discusses the measurement of internal radiation in a CLYC-6 crystal showing that it is at least 50 times smaller than that measured in Ref. [5] for a LaBr3:Ce of equal size. In the successive Section 2.3 the neutron-γ discrimination is discussed. We have focused our attention also on the consequences in the CLYC performances if the UV component of the scintillation light is fully collected (using a quartz window PMT) or if the extremely fast risetime of the scintillation light (in case of γ-rays) is preserved in the measurement by using a timing-fast PMT. In fact, the majority of the published works use a borosilicate window – spectroscopic PMT (usually Hamamatsu 6231-100/6233-100 as for example in Ref. [14,15]). The thermal/fast neutron identification of CLYC-6 and CLYC-7 is described in Section 3. Section 3.1 focuses on thermal neutrons detection pointing out the differences between CLYC-6 and CLYC-7, while Section 3.2 describes the fast neutron detections at 14.1 and 2.5 MeV. The conclusions of the work are described in Section 4.

2. CLYC properties

Two crystals were used in this work: a CLYC enriched at 95% of ^{6}Li (CLYC-6) and a CLYC with an enrichment of ^{7}Li larger than 99% (CLYC-7). Both crystals were produced by RMD and have a cylindrical shape, a diameter of 1″ and a thickness of 1″. For these measurements the CLYC-6 and CLYC-7 scintillators were coupled to HAMAMATSU R6231-100mod PMTs and to standard voltage dividers (HAMAMATSU E1198-26 and HAMAMATSU E1198-27 for CLYC-6 and CLYC-7, respectively).

2.1. Energy resolution

CLYC shows a good energy resolution even though the light yield of ∼20 ph/keV is much smaller than the one of NaI:Tl. Indeed, the CLYC crystal has good energy resolution thanks to the excellent linearity [26] for low deposited energy (E < 100 keV).

The γ-ray energy resolution of the two detectors was measured using a MESYTECK MPR-1 charge integrating pre-amplifier and acquiring the signals with a 12 bit, 600 MHz LeCroy Wave Runner HRO 66Zi oscilloscope. Fig. 1 shows the energy spectra of a ^{137}Cs and a ^{60}Co sources measured with CLYC-6 and CLYC-7. The 662 keV peak produced by the ^{137}Cs source has a FWHM of 32 keV (4.8%) and 30 keV (4.5%), if measured with CLYC-6 and CLYC-7, respectively. The measured energy resolutions are comparable with the RMD datasheets of our two CLYC samples, in which they declare an energy resolution of 5% and of 4.6% for CLYC-6 and CLYC-7 respectively. Similar energy-resolutions values were found in Refs. [9–14] where different crystals, readout and acquisition systems were used.

2.2. Internal activity

The internal activity of the CLYC-6 crystal was measured with and without a Pb shield to discriminate between intrinsic and natural radiation. It is important to remind that the internal radiation is not affected by the lead shield.

In the top panel of Fig. 2, the spectrum measured with the CLYC-6 without shielding (red line) is compared with the spectra measured with 5 cm (blue line) and 10 cm (black line) thick Pb shield. In each measurement, which lasted approximately one week, the data are normalized to the live time. It is evident that the intensity of the measured radiation decreases as the Pb shield increases (except for the thermal neutron peak around 3.2 MeVee).

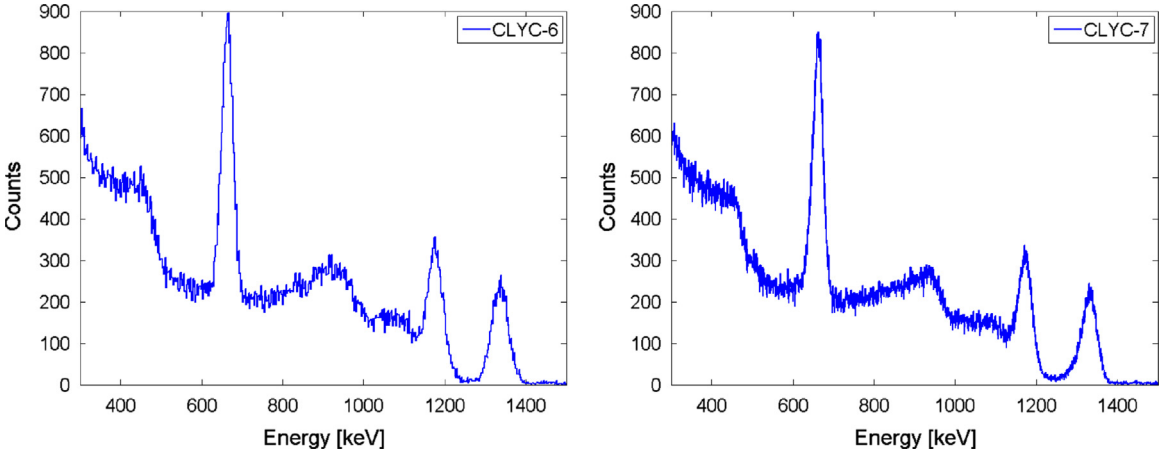

Fig. 1. The energy spectra of two 1″ × 1″ CLYC scintillators using a ^{60}Co and ^{137}Cs sources. The scintillators were coupled to a R6231-100mod Hamamatsu PMT with a standard passive voltage divider (HAMAMATSU E1198-26 and E1198-27). The left-panel shows the spectrum measured with CLYC-6 and the right-panel shows the spectrum measured with CLYC-7.

This suggests that all the other peaks in the top panel of Fig. 3 are from natural background (i.e. ^{40}K, ^{214}Bi, ^{208}Tl).

The neutron peak is located at 3.2 MeV and has the same intensity in all spectra as expected since neutrons are not affected by the Pb shield. In order to highlight the neutron contribution, an AmBe (placed in a 40 cm polyethylene box) thermal neutron source was placed at approximately 2 m from the detector shielded with 10 cm of Pb. The resulting spectrum (magenta line) is compared to the one acquired in the same condition but without the neutron source (black line) in the bottom panel of Fig. 2. The two spectra perfectly overlap, except for the neutron peak which is however very weak as few thermal neutrons, escaping from the polyethylene box, interacts in the CLYC-6 detector which was located at ∼2 m of distance. We could not determinate the origin of the extremely small ($\sim 10^{-4}$ ev/s) thermal neutron flux we measure as background.

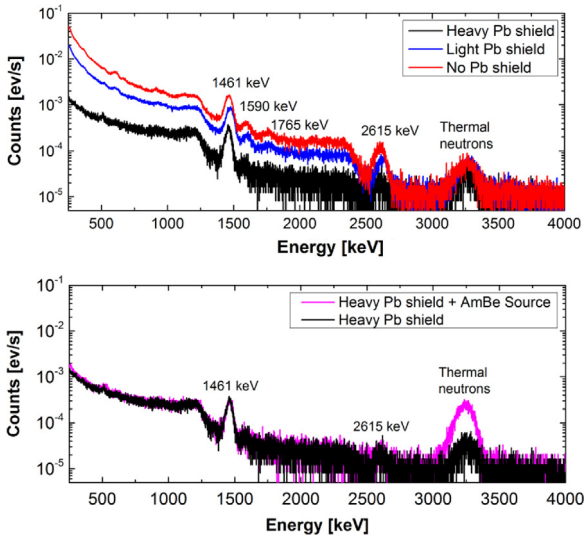

Fig. 2. Upper panel: the internal and natural radiation spectra acquired using three different types of Pb shield. The red spectrum (the one with more counts) was acquired without any Pb shield, the blue and the black spectra were acquired using 5 cm and 10 cm Pb shield, respectively. Bottom panel: the spectra acquired using 10 cm Pb shield with (magenta line) and without (black line) an AmBe thermal neutron source placed approximately 2 m from the detector. (For interpretation of the references to color in this figure legend, the reader is referred to the web version of this article.)

The integral of the spectrum acquired with 10 cm of Pb shield corresponds to a rate of 0.02 cts/s/cm^3. This number is approximately 50 times smaller than what measured in Ref. [5] for a $LaBr_3$:Ce of the same volume and can be considered the upper limit of the internal radiation in CLYC. Such a low internal radiation makes the CLYC crystal a good candidate for low intensity measurements, like, for example, dark matter studies.

2.3. *Neutron and γ discrimination*

The neutron–γ discrimination measurements described in this section were performed using CLYC-6. The possibility to use pulse shape discrimination (PSD) for the identification of the incident radiation is one of the most interesting features of CLYC. Namely, PSD permits to distinguish γ rays and neutrons because of the differences in the scintillation decay response. In particular, since the main difference is in the decay time of the scintillation light of the neutron or γ event, we wanted to investigate whether the use of a timing PMT, having a faster rise time with respect to a spectroscopic PMT, might lead to a better neutron–γ identification. Furthermore, we wanted to study the effect of the CLV component in the signal by comparing PMT's with a borosilicate glass window,

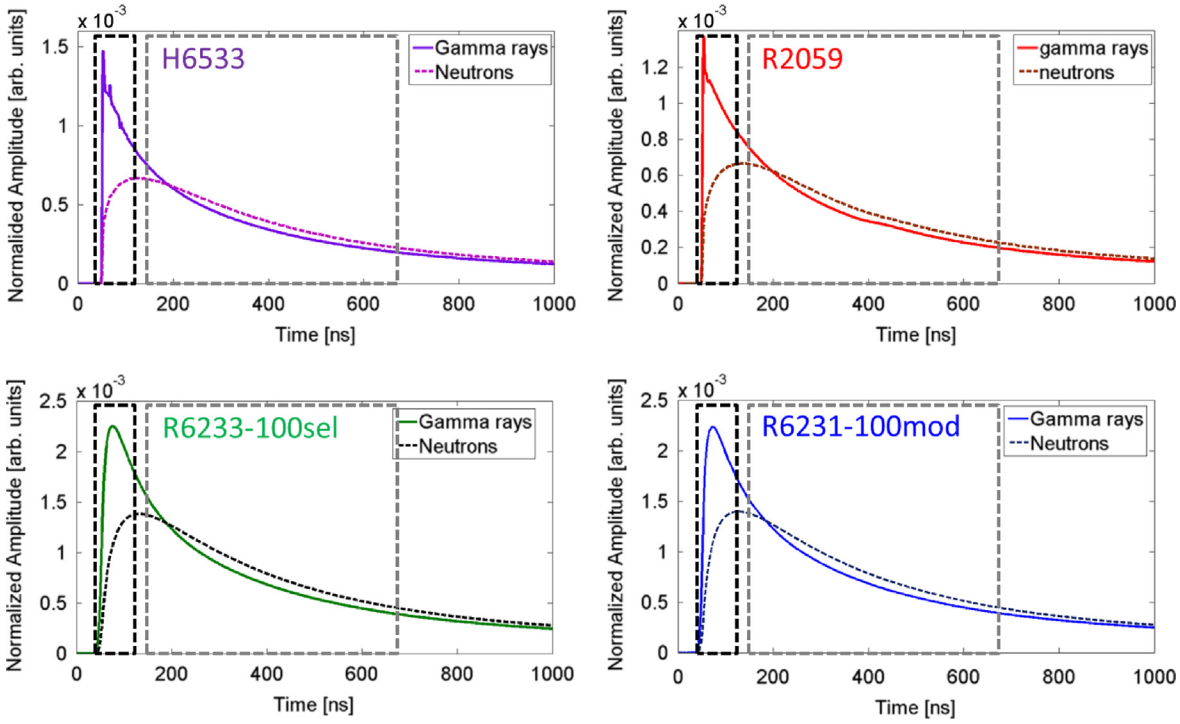

Fig. 3. Comparison between a signal produced by a γ ray and by a neutron using the four different PMTs of Table 1. Top-left panel: the used PMT was H6533 that is a timing PMT with a borosilicate glass window. Top-right panel: the used PMT was R2059 that is a timing PMT with a quarz window. Bottom-left panel: the used PMT was R6233-100sel that is a spectroscopic PMT with a borosilicate glass window. Botton-right panel: the used PMT was R6231-100mod that is a spectroscopic PMT with a quartz window. The two windows W1 and W2, used for the PSD ratio, are indicated with black and gray dashed boxes, respectively. (For interpretation of the references to color in this figure, the reader is referred to the web version of this article.)

which filter about 35% of the CVL light, to PMT's with a quartz window, which detect completely the CVL component. Since the fast component is in the 250–350 nm range (CVL), we might expect a different response to a fast signal in the two cases. Therefore, four different PMT types were tested for neutron–γ discrimination, two timing and two spectroscopic ones with different entrance windows (quartz or borosilicate glass). They are listed in Table 1 together with their properties. The PMT spectral responses are reported in the third column of the table. Note that all the PMTs listed in the table have the maximum of the quantum efficiency (QE) at 420 ns.

The four PMTs were used to detect γ rays from ^{137}Cs, ^{60}Co and thermal neutrons produced by a AmBe source placed in a box of polyetilene. The anode signals were directly sent to the 12 bit, 600 MHz LeCroy waverunner HRO 66Zi oscilloscope and digitized. About 10,000 pulses were averaged to produce the reference pulses for both γ rays and neutrons and are shown in the four panels of Fig. 3, as indicated in the figure legends. The signal properties measured with the different PMTs are reported in Table 2. The timing PMTs, which have a faster intrinsic rise time, show a faster component in the γ-ray signals, while the neutron signals maintain a similar rise time. Following the procedure in literature (see for example Ref. [14]), we set two time windows W1, from the onset of the trace to 80 ns, and W2, from 110 to 660 ns, as indicated in Fig. 3 with black and gray dashed boxes, respectively.

After the integration of the pulses within the two different time windows W1 and W2, we can define the PSD Ratio as

$$\mathrm{PSDRatio} = \frac{W_2}{W_1 + W_2}$$

Since the ratio between the W1 and W2 integrals is different for events relative to γ rays and neutrons, the PSD Ratio allows us to discriminate between γ rays and neutrons event by event. The integral of the signal from the onset up to 3 μs is proportional to the total released energy (W3). By plotting the events in a matrix (PSD matrix) where the *y* axis is the PSD Ratio and the *x* axis is W3 (i.e. the total energy), the neutron events appear clearly separated from the γ-ray ones, as can be seen in Fig. 4.

Table 1
The properties of the HAMAMATSU PMTs used in the measurements as listed in the HAMAMATSU datasheets. The window material, the spectral response, the intrinsic rise time and the blue sensitivity are reported in column 2, 3, 4, and 5 respectively.

PMT	Window material	Spectral response [nm]	Rise Time [ns]	Blue sensitivity index
H6533	Borosilicate glass	300–650	0.7 at 1700 V	10.4
R2059	quartz	160–650	1.3 at 2500 V	11.4
R6233-100sel	Borosilicate glass	300–650	9.5 at 1000 V	15.8
R6231-100mod	quartz	160–650	8.5 at 1000 V	14.0

Table 2
The rise time (10–90% of full signal amplitude) and the fall time (90–10% of full signal amplitude) of the γ-ray and neutron signals measured with the four PMTs of Table 1.

PMT	γ-ray rise time [ns]	γ-ray fall time [μs]	neutron rise time [ns]	neutron fall time [μs]
H6533	2	0.8	30	1.8
R2059	3	0.9	33	1.8
R6233-100sel	17	1.0	40	1.7
R6231-100mod	14	1.0	37	1.7

Selecting the PSD matrix events in the rectangular box of Fig. 4 and projecting them on the *y* axis, we obtain a spectrum with two well separated peaks, one related to neutron events the other to γ-ray events. From the projection it is possible to extract a figure of merit (FOM), defined as:

$$\mathrm{FOM} = \frac{x_{cn} - x_{c\gamma}}{\mathrm{FWHM_n} + \mathrm{FWHM_\gamma}},$$

where x_{cn} and $x_{c\gamma}$ are the centroids of the neutron and γ-ray peaks, while $\mathrm{FWHM_n}$ and $\mathrm{FWHM_\gamma}$ are the FWHMs of the neutron and γ-ray peaks, respectively. The FOM measures the capability of neutron–γ discrimination.

The comparison between the four PMT's was performed in the same conditions: the same windows were chosen and no filter was applied. The resulting FOM values are 2.8, 2.9, 3.4 and 3.2 for H6533, R2059, R6233-100sel and R6231-100mod, respectively, with an estimated standard deviation of 0.1. Note that a FOM value of 1.5 provides a rejection ratio better than 10^6 (in the case of ideal Gaussian shapes of the projected peaks) [28]. It is important to point out that the typical rejection ratio of ^{3}He detector is of the order of 10^6 [10]. From this comparison, we see that all tested PMTs give a good neutron–γ discrimination. The obtained FOM values show that the effect of quartz or borosilicate windows is too small to be observed, which might not be surprising since only about 35% of the CVL light is filtered by the borosilicate window. We also note that the spectroscopic PMT's give a slightly better FOM than the others PMTs. This is somehow unexpected as, due to the fast rise-time of a timing PMT, one might hope that the timing PMT's produce a better discrimination between neutrons and γ events which might compensate for the worse energy resolution. Since the major difference between the timing and spectroscopic signals is in the first 10 ns, we also tried to reduce the time window length, considering the maximum in the first 5 ns (M1) and the integral of a 5 ns window at 300 ns after the signal onset (M2). The ratio M1/M2 between neutrons and γ-rays averaged pulses is much higher for timing PMTs than for the others. However, on an event by event basis, we found that, for timing PMTs, the FOM value (see equation 1) reduces to ~2, due to the fact that the pulse shape is less defined than in spectroscopic PMT's. The fact that the spectroscopic PMTs produce a better FOM may be ascribed to the longer intrinsic rise time than the timing PMTs (see Table 1). This, acting as a low pass filter, reduces the high frequency noise.

Even though one could use/define more complicated and "ad hoc" algorithms which take advantage on the γ-rays induced fast rising signal, we conclude that, using a simple algorithm, spectroscopic PMT's give a better neutron–γ discrimination compared to timing PMT's. In addition, the energy resolution at 662 keV, measured from the W3 values, produced the values: 5% for both the spectroscopic R6233-100sel and R6231-100mod PMTs, 7.2% for H6533 and 6.6% for R2059 PMTs.

As we have noticed that the removal of very high frequency noise might improve the FOM, we have also filtered the signals produced by the R6231-100mod PMT coupled to CLYC-6. In particular, a signal smoothing was applied (low pass filter) to improve the signal to noise ratio. Moreover a window W1 of 70 ns was used and a 100 MHz filter was applied to optimize the FOM value. The PSD ratio vs γ-rays energy matrix and its projection are shown in the left panel of Fig. 5. The two peaks corresponding to neutron and γ-ray events are shown in the right panel of Fig. 5. In this case it was possible to obtain a FOM value of 3.8.

FOM values, ranging from 1 to 4.8 are reported in Refs. [14,26,27]. They are from different CLYC samples, calculated in different energy ranges. The FOM values found in this work (from 2.8 to 3.8) agree with the reported values. It is important to point out that the FOM value depends on several parameters like the energy range of the neutrons, the count rate, the used algorithm,

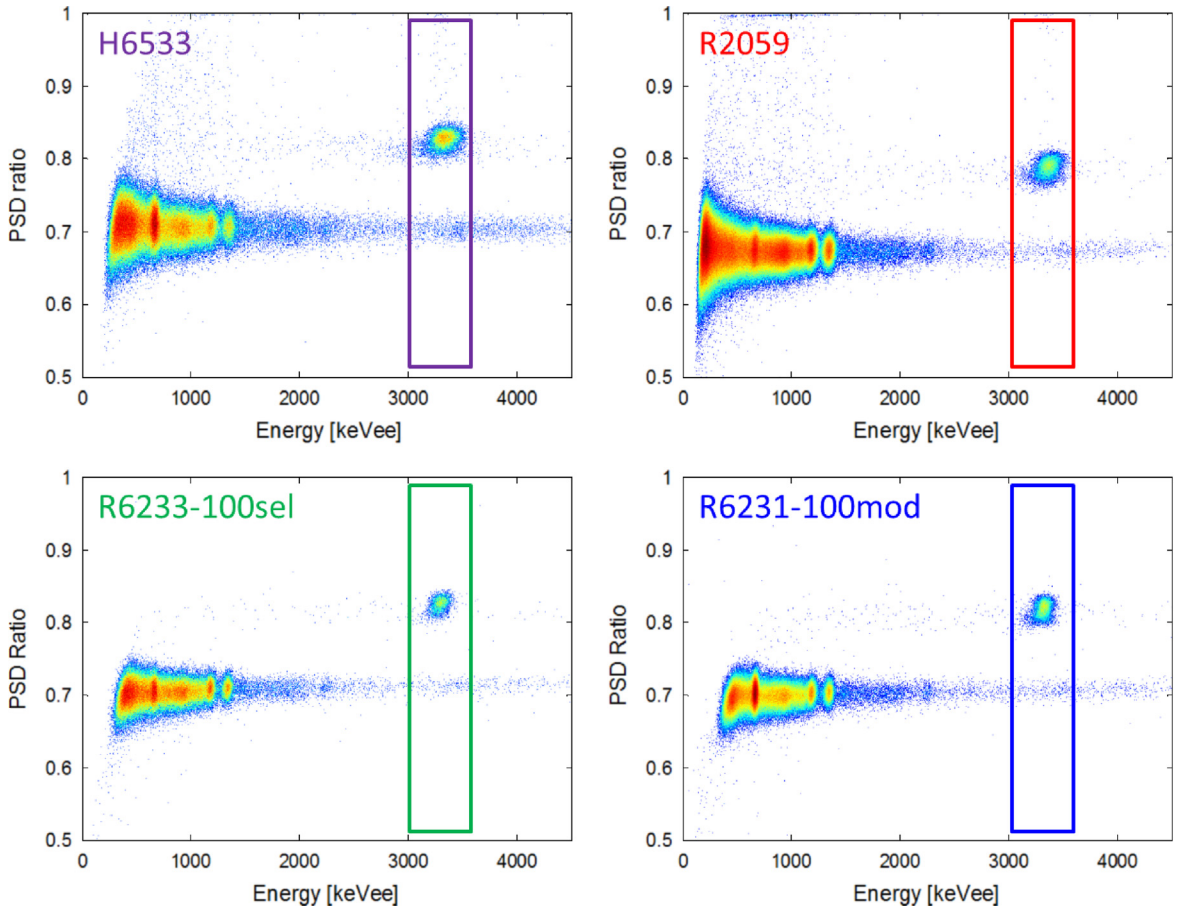

Fig. 4. The PSD matrices for the four different PMTs of Table 1. Top-left panel: the used PMT was H6533 and a FOM of 2.8 was found (see text). Top-left right: the used PMT was R2059 and a FOM of 2.9 was found. Bottom-left panel: the used PMT was R6233-100sel and a FOM of 3.4 was found. Botton-right panel: the used PMT was R6231-100mod and a FOM of 3.2 was found.

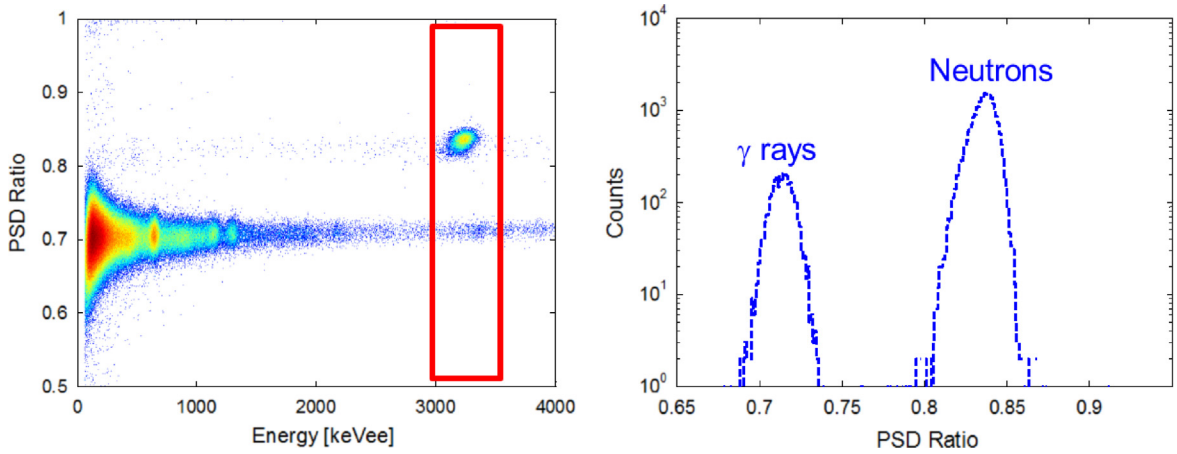

Fig. 5. Left panel: the PSD matrix of CLYC-6 obtained using the HAMAMATSU R6231-100mod PMT and a digital filter (see text). In the matrix plot the *z*-axis is in logarithm scale. Right panel: The projection of the red box along the *y* axis of the PSD matrix. The measured FOM is 3.8. (For interpretation of the references to color in this figure legend, the reader is referred to the web version of this article.)

the filters applied on signals and so on. The highest FOM value found in literature, 4.8, [14], was found after an optimization of the pulse shape algorithms.

3. Neutron identification

For the following measurements, the CLYC-6 and CLYC-7 scintillators were used. They were coupled to HAMAMATSU R6231-100mod PMTs and to standard voltage dividers (HAMAMATSU E1198-26 and HAMAMATSU E1198-27 for CLYC-6 and CLYC-7, respectively). Data were taken with a 12 bit LeCroy Wave Runner oscilloscope (HDO ZI66).

3.1. Thermal neutron detection

The thermal detection capability arises from ^{6}Li ions, which have a 940 barns cross-section for the reaction ^{6}Li (n, α)^{3}H.

Thermal neutrons were measured with both CLYC-6 and CLYC-7 crystals. The only difference between the two crystals is the Li isotope enrichment. In particular, as already mentioned, our CLYC-6 detector has an enrichment of 95% of ^{6}Li, while the CLYC-7 crystal has an enrichment of ^{7}Li higher than 99%, and is expected to be insensitive to thermal neutrons. In Fig. 6 the comparison between the energy spectra measured with the CLYC-6 (blue line) and the CLYC-7 (red line) detectors is shown. Both detectors were placed over a 40 cm box of polyetilene with a source of AmBe in the center. The spectra of Fig. 6 are normalized on the ^{137}Cs peak. The 3.2 MeVee peak, induced by thermal neutrons, clearly visible in CLYC-6 spectrum, is absent in the CLYC-7 one. The FWHM of the thermal-neutron peak is 3.2% for the CLYC-6 sample. The PSD matrix confirms the different sensitivity to thermal neutrons of CLYC-6 and CLYC-7, as shown in Fig. 7. The spot produced by thermal neutrons, which is present only in the CLYC-6 matrix, is clearly visible at PSD $\sim$0.8 and E=3.2 MeVee. The sensitivity ratio, calculated as the ratio between the events present in CLYC-6 and in CLYC-7 matrix in the region $3.0 < x < 3.5$ MeV and $0.76 < y < 0.81$, is 391 ± 78. Consequently, we can conclude that the CLYC-7 detector has an efficiency to thermal neutrons less than $\sim$0.3% with respect to the CLYC-6 one. Assuming that the thermal neutron sensitivity comes only from ^{6}Li nuclei we can extract a ^{6}Li concentration in CLYC-7 crystal of 0.26 ± 0.05%. This value is consistent with what declared in the datasheets by RMD.

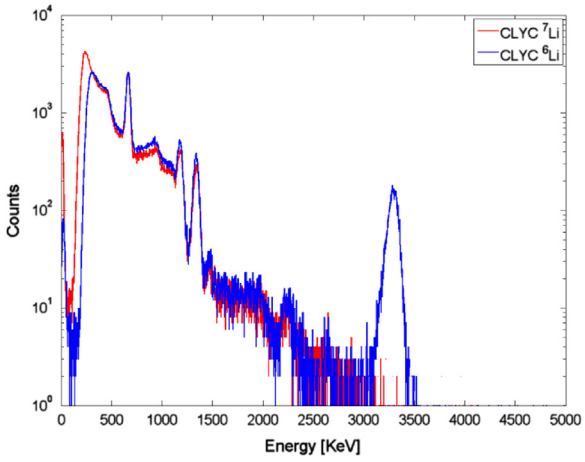

Fig. 6. Spectra measured with a CLYC-6 and CLYC-7 placed near AmBe source in a polyethylene box with side of 40 cm. The spectra were taken sequentially. The sources and the crystals were in the same position for both measurements. Both crystals were coupled to a R6231-100mod PMT, E1198-26 and E1198-27 VD for CLYC-6 and CLYC-7 respectively and powered at 1000 V. The energy thresholds in the two spectra were slightly different. (For interpretation of the references to color in this figure, the reader is referred to the web version of this article.)

3.2. Fast neutron detection

Fast neutrons are detected exploiting the reactions ^{35}Cl(n, p)^{35}S and ^{35}Cl(n, α)^{32}P. The energy of the outgoing proton or α particle is linearly related to the neutron energy. For this reason, CLYC scintillators are neutron spectrometers. Furthermore, the neutron kinetic energy can also be measured via the Time of Flight technique (FWHM < 1 ns) [14].

A measurement was performed at the Neutron Generator at ENEA laboratories in Frascati (Italy), which provided 14.1–2.5 MeV neutrons.

The 14.1 MeV neutron emission was obtained bombarding a tritium doped titanium target with a 300 keV deuterium beam [29]. The two samples of CLYC scintillators were placed at 1.25 m from the neutron source, as the flux was very high. The neutron generator of ENEA produced a neutron yield of $5 \cdot 10^{8}$ n/s. It was measured by the standard neutron counting diagnostic, which consists of an absolutely calibrated detector measuring alpha particles produced by deuterium–tritium reactions in the target. We use the same set up and the same beam of Ref. [7]. The neutron generator is at 4.5 m from the floor and walls, to reduce the thermal neutron background. Both CLYC detectors were used for the measurement of 14.1 MeV neutrons.

The left and right panels of Fig. 8 show the PSD matrices obtained with 14.1 MeV neutrons measured in CLYC-6 and in CLYC-7, respectively. In both cases, the discrimination between γ rays and neutrons is clearly visible. The thermal neutron peak is present only in the left panel of Fig. 8 at about 3.2 MeVee. In the figure, the neutron events show two components probably due to protons and α particles produced by the two reactions on ^{35}Cl as suggested in Ref. [15]. In this case the neutron contribution appears as a continuum without any distinct peak. This feature may be connected to both the different two-three-body reactions that may occur with neutrons of 14.1 MeV and the fact that the

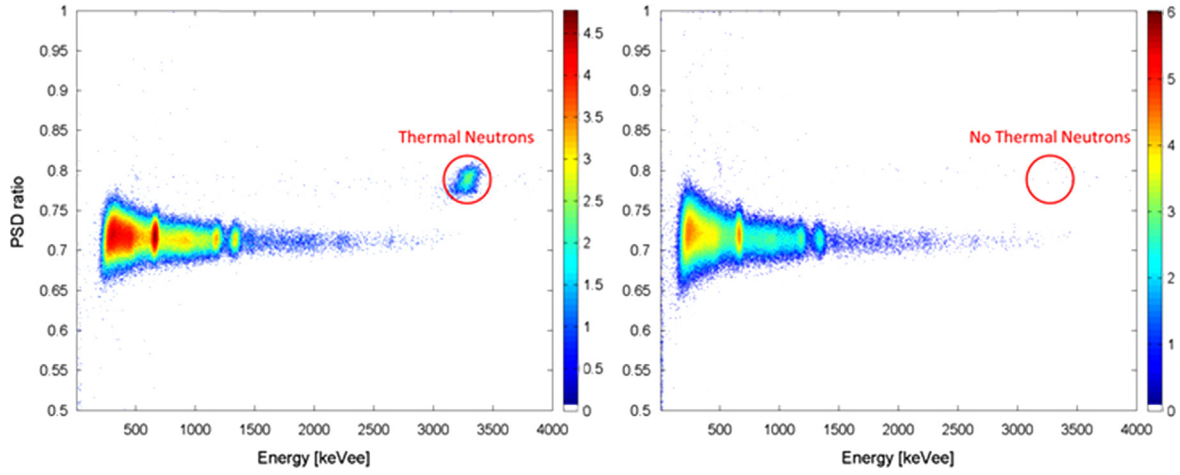

Fig. 7. The PSD vs energy 2D matrices of CLYC-6 (left panel) and CLYC-7 (right panel). The z-axis is in logarithm scale. The plots show the capability to identify neutrons and γ rays in a CLYC scintillator. In the x axis there is the measured energy (electron equivalent) while in the y axis there is the PSD ratio (see text). The circle indicates thermal neutrons.

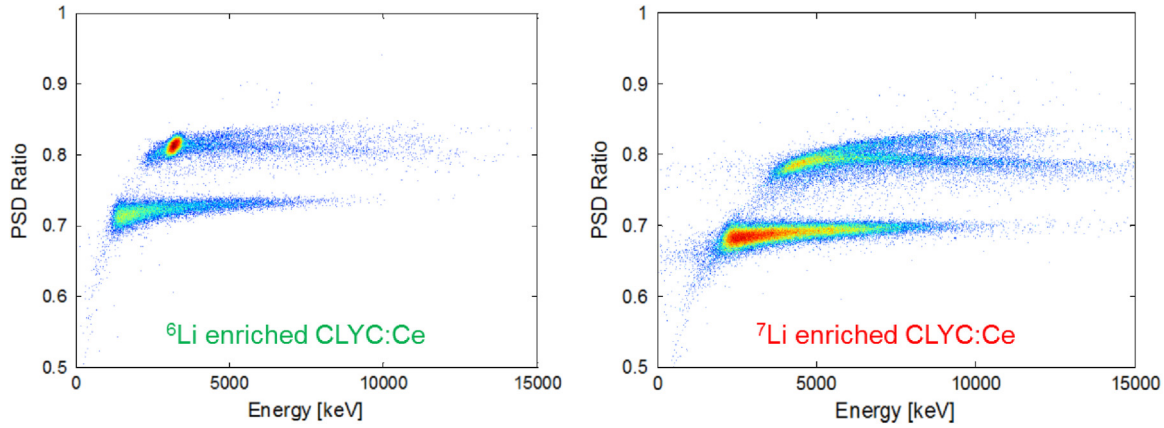

Fig. 8. The PDS matrixes obtained with fast neutrons of 14.1 MeV. Left panel: the matrix obtained with CLYC-6, thermal neutron are evident as a spot located at $x \sim 3200$ and $y \sim 0.8$. Right panel: the matrix obtained with CLYC-7. The z axis is in log scale.

final nucleus might also be left in an excited state. At this energy, several three-body channels are open with a cross-section even 10 times larger than the neutron capture on ^{35}Cl. For example, the cross-section of ^{133}Cs(n, 2n)^{132}Cs is ~1.5 barns whereas the cross-sections of ^{35}Cl(n, p)^{35}S and ^{35}Cl(n, α)^{32}P at 14.1 MeV is ~0.15 barns only [22,24].

The continuum spectrum for neutrons with energy larger than 8 MeV was already observed by D'Olympia et al. [15]. They performed a simulation including all possible reactions on ^{35}Cl and found that the major contribution is given by protons and α particles, while no tritons or deuterons are expected to be produced by neutron induced reactions at these energies. The comparison between data and simulations was reasonably good, although the contributions of other neutron induced reactions cannot be excluded. A more detailed study of the emitted particles should be performed to understand which reactions are involved. The matrix shows also gamma events as in Ref. [15,24]. These gamma rays could be due to background or prompt and delayed decays of nuclear excited states populated in the neutron induced reactions.

The 2.5 MeV neutrons were produced by the primary beam impinging on the beam dump, containing deuterium atoms. For this reason, the flux of the 2.5 MeV neutrons was weaker and less monochromatic than the flux of the 14.1 MeV neutrons. In this case the energy of the thermal peak is expected to overlap with the proton energy produced by the ^{35}Cl(n, p)^{35}S reaction, because of the Q-value of the reaction, 0.6 MeV, to be added to the neutron energy. Since the CLYC-7 crystal is almost not sensitive to thermal neutrons, as discussed in Section 3.1, the 2.5 MeV neutrons were detected using only this crystal. At this incident energy, the reaction ^{35}Cl(n, α)^{32}P is expected to have an almost negligible cross-section to be observed [22–24]. Fig. 9 shows the resulting PSD matrix. The counts in the red circle, where the neutron events are expected, are ~700. A comparison with the CLYC-6 detector taking into account the 0.3% efficiency factor discussed in Section 3.1 make us to estimate a maximum of ~13 thermal neutron events in Fig. 9.

Previous measurements of monochromatic neutrons in this energy range are reported in Refs. [15,24]. In particular, in Ref. [24] a CLYC-6 crystal was used to detect 2.58 MeV neutrons, while 2.01 and 2.69 MeV neutrons were detected by a CLYC-7 in Ref. [15]. Our results well compare with what found in both references, although in Ref. [24] the presence of the thermal neutron peak partly overlaps with the fast neutron peak.

In our case, the FWHM of the proton peak is dominated by the spread in the incident neutron energy and cannot therefore be compared with that observed in [15,24] where a monochromatic beam was used.

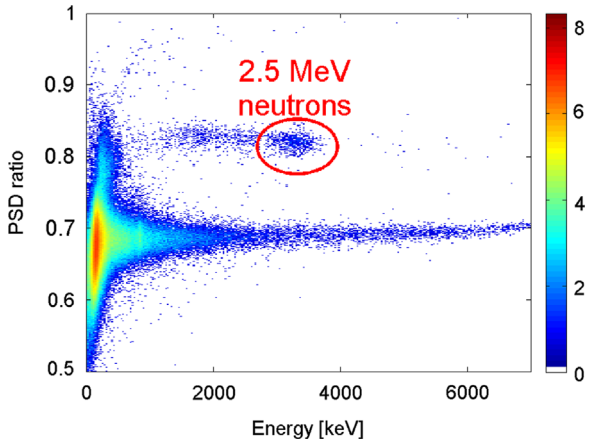

Fig. 9. The PDS matrix obtained with fast neutron of 2.5 MeV measured with CLYC-7 scintillator. The neutron peak, related to reaction ^{35}Cl(n, p)^{35}S is indicated by the circle. (For interpretation of the references to color in this figure legend, the reader is referred to the web version of this article.)

4. Conclusions

In this work, we presented the results from the investigation of the performances of two 1″ × 1″ samples of CLYC scintillator: one enriched with 95% of ^{6}Li (CLYC-6) and the other with an enrichment of ^{7}Li larger than 99% (CLYC-7). The CLYC scintillators exhibit good energy resolution under γ-ray excitation. We measured 4.8% and 4.5% at 662 keV for CLYC-6 and CLYC-7, respectively. An important property of these scintillators is the capability to identify and measure γ rays and neutrons via pulse shape discrimination. We studied the signals produced by spectroscopic PMTs, by timing PMTs (which preserve the fast rise-time of the scintillation light) and quartz windows PMTs (which are sensitive to the UV component of the scintillation light). We have observed that the FOM for n–γ discrimination, using the simple algorithm suggested in literature, is better for spectroscopic PMTs. The FOM value of 3.8 was found for thermal neutrons using a HAMAMATSU R6231-100mod PMT after filtering the signals. We also measured the CLYC internal radiation and we have found that it is at least two orders of magnitude smaller than that of an equivalent $LaBr_3$:Ce detector.

The thermal neutrons, produced by an AmBe source surrounded by polyetilene, were measured with both detectors. It was observed that the thermal neutron detection efficiency for the CLYC-7 is less than 0.3% with respect to the CLYC-6 sample. This value is consistent with what declared in the reference sheet of

RMD (concentration of $^{7}Li > 99\%$). In order to test the capability of these crystals to detect fast neutrons, an experiment was performed at the Frascati Neutron Generator facility (Italy). A deuterium beam was used to provide neutrons of $\sim$2.5 MeV or 14.1 MeV, respectively. We found a peak related to 2.5 MeV neutrons and a continuum energy spectrum for 14.1 MeV neutrons, due to a superimposition of different reaction mechanisms.

Acknowledgments

This work was supported by *NuPNET - ERA-NET* within the NuPNET GANAS Project, under grant agreement No. 202914 and from the European Union, within the "7th Framework Program" FP7/2007-2013, under grant agreement No. 262010 – ENSAR-INDESYS. This work was also supported by "Programmi di Ricerca Scientifica di Rilevante Interesse Nazionale" (PRIN) No. 2001024324_01302.

References

[1] A. Giaz, et al., Nucl. Instrum. Methods A. 804 (2015) 212.
[2] "BrilLanCe Scintillators Performance Summary.pdf" available at ⟨http://www.detectors.saint-gobain.com/Brillance380.aspx⟩.
[3] O. Guillot-Noël, et al., J. Lumin. 85 (1999) 21.
[4] E.V.D. Van Loef, et al., Appl. Phys. Lett. (79) (2001) 1574.
[5] R. Nicolini, et al., Nucl. Instrum. Method A 582 (2007) 554.
[6] A. Giaz, et al., Nucl. Instrum. Method A 729 (2013) 910.
[7] C. Cazzaniga, et al., Nucl. Instrum. Method A 778 (2015) 20.
[8] M. Ciemala, et al., Nucl. Instrum. Method A608 (2009) 76.
[9] J. Glodo, et al., IEEE Trans. Nucl. Sci. 55NS (2008)1206 and IEEE Trans. Nucl. Sci. 56NS (2009)1257.
[10] J. Glodo, et al., IEEE Trans. Nucl. Sci. 58NS (2011) 333.
[11] J. Glodo, et al., J. Cryst. Growth 79 (2013) 73.
[12] B.S. Budden, et al., IEEE Trans. Nucl. Sci. 60NS (2013) 946.
[13] M.B. Smith, et al., Nucl. Instrum. Method A784 (2015) 162.
[14] N.D'Olympia, et al., Nucl. Instrum. Method A714 (2013) 121.
[15] N.D'Olympia, et al., Nucl. Instrum. Method A763 (2014) 433.
[16] K. Yang, P. Menge, Nucl. Instrum. Method A784 (2015) 74.
[17] R. Machrafi, et al., Radiat. Meas. 70 (2014) 5.
[18] N. Cherepy, et al., IEEE Trans. Nucl. Sci. 60NS (2013) 955.
[19] F. Quarati, et al., Nucl. Instrum. Method A 729 (2013) 596.
[20] R. Billnert, et al., Nucl. Instrum. Method A 647 (2011) 94.
[21] N. Cherepy, et al., Nucl. Sci. Symp. Med. Im. Conf. (NSS /Mic.) (2012) 1692–1697.
[22] Pointwise ENDF-VII library at 300 K: ⟨http://atom.kaeri.re.kr⟩.
[23] D'Olympia, et al., Nucl. Instrum. Method A694 (2012) 140.
[24] M.B. Smith, et al., IEEE Trans. Nucl. Sci. 60NS (2013) 855.
[25] RMD - ⟨http://rmdinc.com/clyc/⟩.
[26] D.W. Lee, et al., Nucl. Instrum. Method A664 (2012) 1 , and references therein.
[27] M. Martone, M. Angelone, M. Pillon, J. Nucl. Mater. 212 (1994) 1661.
[28] A. Winyard, et al., Nucl. Instrum. Method A95 (1971) 141.
[29] ⟨www.fusione.enea.it/LABORATORIES/Tec/FNG.html.it⟩.